Available online at www. jbr-pub.org

Open Access at PubMed Central

JBR

The Journal of Biomedical Research, 2013, 27(6):495–508

Research Paper

Individual differences in transcranial electrical stimulation current density

Michael J Russell[a,✉], Theodore Goodman[b], Ronald Pierson[c], Shane Shepherd[d], Qiang Wang[a], Bennett Groshong[a], David F Wiley[e]

[a]*Aaken Research Institute, Inc. Davis, CA 95616, USA;*

[b]*Sutter Center for Psychiatry, Sacramento, CA 95826, USA;*

[c]*Brain Image Analysis, LLC Los Angeles, CA 90012, USA;*

[d]*Radiological Associates of Sacramento, Inc. Sacramento, CA 95816, USA;*

[e]*Stratovan, Corp. Sacramento, CA 95826, USA.*

Received 08 May 2013, Revised 16 July 2013, Accepted 28 July 2013, Epub 25 October 2013

Abstract

Transcranial electrical stimulation (TCES) is effective in treating many conditions, but it has not been possible to accurately forecast current density within the complex anatomy of a given subject´s head. We sought to predict and verify TCES current densities and determine the variability of these current distributions in patient-specific models based on magnetic resonance imaging (MRI) data. Two experiments were performed. The first experiment estimated conductivity from MRIs and compared the current density results against actual measurements from the scalp surface of 3 subjects. In the second experiment, virtual electrodes were placed on the scalps of 18 subjects to model simulated current densities with 2 mA of virtually applied stimulation. This procedure was repeated for 4 electrode locations. Current densities were then calculated for 75 brain regions. Comparison of modeled and measured external current in experiment 1 yielded a correlation of r = .93. In experiment 2, modeled individual differences were greatest near the electrodes (ten-fold differences were common), but simulated current was found in all regions of the brain. Sites that were distant from the electrodes (e.g. hypothalamus) typically showed two-fold individual differences. MRI-based modeling can effectively predict current densities in individual brains. Significant variation occurs between subjects with the same applied electrode configuration. Individualized MRI-based modeling should be considered in place of the 10-20 system when accurate TCES is needed.

Keywords: MRI, modeling, current density, transcranial-stimulation, tDCS

INTRODUCTION

Transcranial electrical stimulation (TCES) is an established therapy for a number of clinical conditions that range from major depression[1-4] to tinnitus[5-7]. TCES is able to induce neuroplastic changes[8,9], excitability shifts[8,10] and evoked responses[11] that are dependent on the type, duration and polarity of electrical stimulus. High intensity stimuli and pulse trains are extensively used in surgical neuromonitoring[11-13] and psychiatry[14-16]. Low intensity direct current (transcranial direct current stimulation (tDCS)) and alternating current TCES are less well established, but have gained recognition as treatments for: chronic pain[17,18],

✉Corresponding author: Dr. Michael J Russell, Aaken Research Institute, 216 F Street Suite 76, Davis, CA 95616, USA. Tel: 1+530-661-0446, E-mail: mrussell@aakenlabs.com.

The authors reported no conflict of interests.

doi:10.7555/JBR.27.20130074

memory enhancement[19,20], epilepsy treatment[21] and a variety of other conditions as a way for modulating cortical excitability. Direct current applied to neural tissues can initiate stem cell recruitment[22,23] and somatic cell migration[24-26], or modify blood perfusion[27] TCES of alternating current at specific frequencies has been shown to inhibit metastatic spread of tumors[28] without the side effects that occur with surgery, radiation, or chemotherapy. These applications of TCES have had remarkable success in individual studies, but often exhibit significant failure rates when applied to broad populations[29].

Effective use of an electrical stimulus for neuromodulation depends on 5 factors: polarity, duration, waveform, targeting and current density. Polarity, duration and waveform are easily manipulated with modern electronics and the resulting signal is either direct current (DC), pulsed, or alternating. Managing the location of electrical energy and its intensity in brain tissues has been more problematic.

TCES targeting is usually achieved by placing electrodes on the scalp directly "over" the intended brain region by using the 10-20 system. Stimulus intensity delivered to this region has been estimated from the amount of current leaving the electrodes. This method has significant limitations because the head and brain are comprised of varying resistivities with complex and individual unique anatomies, while the 10-20 system is based on a normalized anatomy. Nevertheless, this method has been persistently used for determining stimulation location for the lack of a better alternative. However, it is critical for treatment success to have an accurate understanding of the current that is actually delivered to a targeted brain region. Recognizing this problem, investigators have relied on simulations to provide contributions to our understanding, but these simulations have had critical limitations. Previous studies (including ours) have focused on either a single-slice of the head[30] , a single subject[31-34] or simplified anatomic models of cranial components[35-37]. These studies have led to improvements in the understanding of neural modeling, but not resolved the problem of individual anatomic variation in the normal population nor do they address the greater anatomic variations seen in patient populations with tumors, strokes, trauma and etc. An improvement in the ability to predict the intensity of an electrical stimulus at a region of interest will likely result in improvements in electrical stimulation outcomes.

The modeling discussed in this paper attempts to resolve the issues by using magnetic resonance imaging (MRI) techniques to create a measurement of the amount of hydrogen atoms in a tissue. MRIs are typically used to create images but can also be used to make measurements. This study is based on a hypothesis that is conceptually simple but computationally complex. The concept is that MRIs represent the amount of hydrogen in a tissue[38] (principally water) and tissue resistivity is primarily determined by the amount of water in tissue[39]. Based on this principle, we hypothesized that MRIs can be converted to a conductivity index and act as the foundation for electric current simulation.

The present study compared exact models of subjects´ heads created from MRIs to evaluate the expected individual differences in current density distribution throughout each head when electrodes are placed at 4 identical locations determined by the traditional 10-20 system.

MATERIALS AND METHODS

This study protocol was approved by the institutional review board of the Sutter Institute for Medical Research, Institutional Review Board. Participating individuals gave fully informed consent.

MRI procedures

To map the conductivity of brain tissue, a three-dimensional (3-D) measurement of the hydrogen distribution in head and brain is needed rather than the typical individual MRI record. T1, T2 and proton density (PD) imaging each captures different aspects of the water (hydrogen) present in tissues, but each alone lacks the power to provide a precise brain conductivity model (***Fig. 1***). To get a more precise picture, T1, T2 and PD recordings of the entire head above the maxilla were first combined to model the isotropic conductivity, then diffusion weighted recording by the volume constrain technique[40] was performed to account for anisotropic conductivity; magnetic resonance angiography (MRA) was performed to account for the increased conductance through blood vessels.

MRIs that are a 3-D measurement of the hydrogen in a tissue were needed rather than the typical imaging recordings (e.g. T1, T2, or positron density). To map tissue´s conductivity, multiple 3T MRI recordings of the entire head above the maxilla were obtained from each subject. T1, T2 and positron density recordings each captured different aspects of the water (hydrogen) present in tissues, but without sufficient power to differentiate tissue types so they were combined to provide better definition (***Fig. 1***). Additionally, diffusion weighted recordings were performed to account for anisotropy and, and MRA to account for conductance through blood vessels. The slices spanned the head from its apex to approximately the roof of the mouth

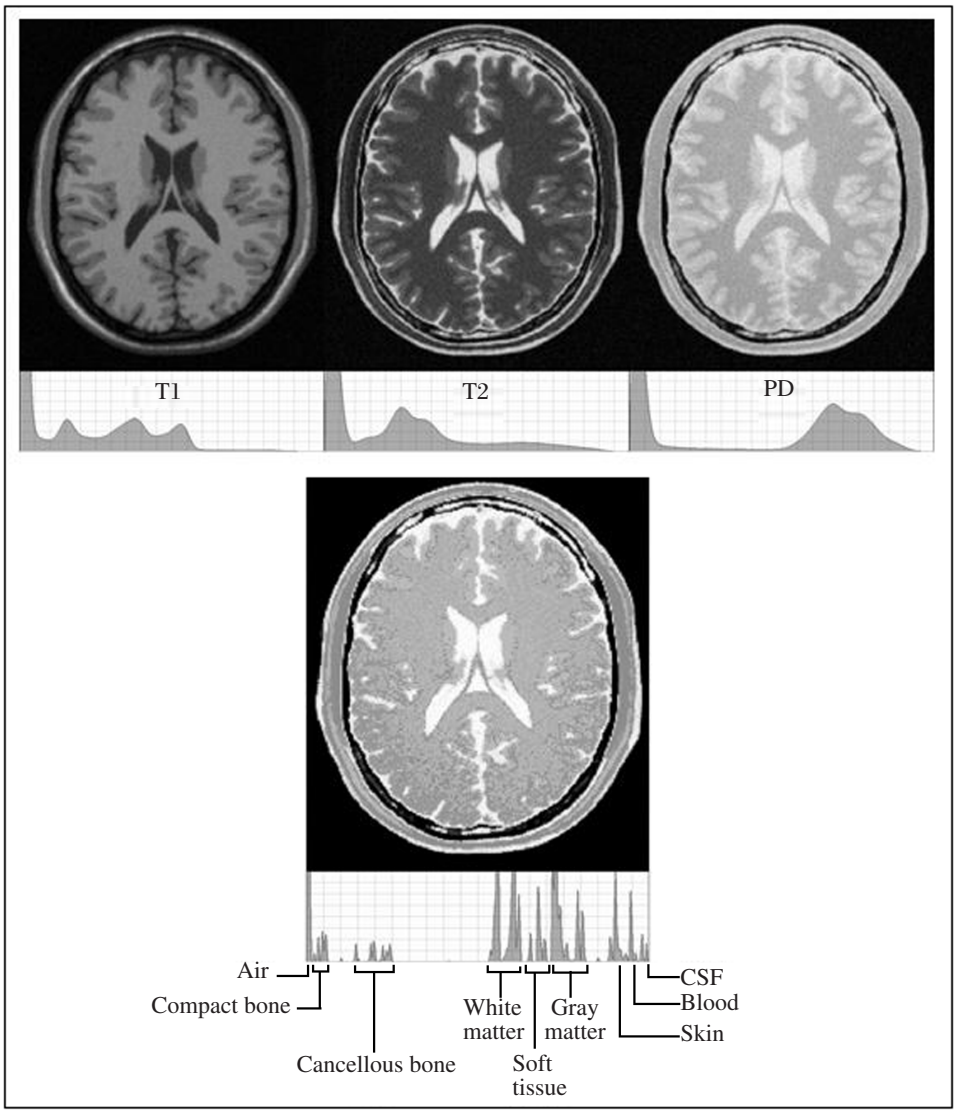

Fig. 1 **The top row is MRIs with gray scale density graphs for each of T1, T2 and proton density images.** The bottom image is a combination of the above images with a gray scale density graph below it. Note the segmentation of tissues in the histogram of the combined image not seen in T1.T2, or PD.

and included the ears. The recordings were obtained on a General Electric MRI (Discovery M750) machine with a 1 mm by 1 mm pixel by 1 mm slice spacing. Diffusion weighted recordings were taken at 2 mm by 2 mm pixel by 2 mm slice spacing. This combination of MRIs constitutes the Aaken Insite Protocol[41]. Image data were combined into a single 3-D representation and a conversion equation was applied to achieve an index of resistivity, yielding the subject´s resistivity model. The resistivity to the MRI pixel intensity is expressed by the formula:

$$R(v) = K(1\text{-}v)^{E} + D \quad (1)$$

Where v ϵ[0,1] is the normalized intensity of the combined image at the given voxel; R is the resistivity; K=16,000; E=4 and D=65 are the adjustable parameters. This formula and the parameters were empirically derived[41].

Calibration

MRI images varied in intensity and were obtained on a gray scale. To control for these variations in the intensity and density of each MRI recording, it was necessary to establish high and low gray scale calibration points for each image. This was done by using the air around the head as the highest resistivity value (5 million Ohms per cm) and the subject´s cerebral spinal fluid (65 Ohms per cm) as the low value. By using this technique, the subject´s images were normalized and then combined into a single 3-D rendering. MRA image of blood vessels was performed to account for

the conductivity of moving blood in vessels during recording which would otherwise show up as a high resistivity region. Moving blood is a good conductor, but tends to appear as a dark image (poor conductor) in the static MRIs.

Finite element and boundary conditions

The subject´s resistivity distribution was then translated to a rectangular prismatic linear finite element model. The model matrix equation and boundary conditions were formulated from the Galerkin equations[42]. Solutions to the system matrix equations were obtained by using the conjugate gradient method[43].

Finite element meshing

It was assumed that current densities could be predicted by using a quasi-static electrical model and that low frequency and DC TCES would produce similar results. The finite element models solved the Laplace equation

$$\nabla \cdot [\sigma(x,y,z) \nabla \Phi] = 0 \quad (2)$$

on the domain (the head), subject to

$$\sigma \frac{\partial \Phi}{d\mathbf{n}} = j \text{ and } \sum_{d\Omega} j = 0 \quad (3)$$

where dΩ is the head surface, Φ is the voltage distribution, j is the current density at the surface and n is a vector normal to the surface. The quantity $\sigma(x,y,z)$ is the conductivity distribution within the head (the reciprocal of the resistivities estimated from MRI data). The finite element model meshing matrix equations were formulated for rectangular prismatic elements directly from the Galerkin equation[42]. The resulting mesh consisted of approximately 11.5 million elements for each subject. Calculations were implemented in C++. Diffusion tensor vectors defined on the model were performed to extend anisotropic conductivity to white matter voxels. In each white matter voxel, the anisotropic conductivity tensor was calculated as

$$\mathbf{D}_W = \mathbf{A}^T \mathbf{D}^*_W \mathbf{A} \quad (4)$$

Where:

$$\mathbf{D}^*_W = \begin{bmatrix} \sigma_l & 0 & 0 \\ 0 & \sigma_t & 0 \\ 0 & 0 & \sigma_t \end{bmatrix}$$ and $\mathbf{A} = \mathbf{R}_Z \mathbf{R}_Y \mathbf{R}_X$, where $\mathbf{R}_Z$, $\mathbf{R}_Y$, and $\mathbf{R}_X$ are rotation matrices about the *z*, *y*, and x axes, respectively. Matrix equations were solved in Matlab (2009b) via a sparse matrix version of the preconditioned conjugate gradient method that used diagonal of the stiffness matrix as the preconditioning matrix. Both isotropic and anisotropic models were verified against an analytic solution for a cube before we began analyzing brain model results.

Current densities within the models were determined from the finite element model solution by calculating current densities for each voxel.

$$\mathbf{J} = D_W \nabla \Phi \quad (5)$$

Experiment 1: validation

In this first study, simulated current densities were calibrated to surface measurements. Three of the authors volunteered (males between the ages of 35-68) to validate the model by determining the accuracy of the modeling by establishing a correlation of the model as compared to surface measurements from the head during stimulation. Stimuli for the recordings were a square wave train of 1,000 microseconds. pulses, at 0.1 mA. To cancel out any potential 60Hz electrical noise that might be present in the environment, a stimulation rate of 3.11 cycles per second was selected. Electrodes for stimulation were silver-silver chloride hydrogelled 0.75 in pads (Ambu, Ballerup, Denmark). Recordings were made with a signal averaging machine (Cadwell Cascade, Kennewick, WA, USA) and averaged for 10 pulses. Positions on the head (***Fig. 2***) were obtained with a microscribe (Immersion Microscribe 3DX, Amherst, VA, USA). The microscribe is a point to point mechanical arm that is able to measure and locate points in 3-D spaces with an accuracy of 0.2 mm. Measurement locations were virtually registered in software with the conductivity model and simulations were run for each subject. Virtual voltage samples were collected from the simulation prediction results at the 25 real-world sampled locations (***Fig. 2***, where green is the ground, red is the stimulating and blue is the recording electrodes). Pearson R correlations were computed between the predicted and measured voltages for the subjects. The measured locations were recorded with a sharp-pointed stainless steel recording tip attached to the microscribe. To insure the accurate placement of the microscribe, and to control head movement that might normally occur during the recording procedure, the subjects lay on a table in the supine position. The head was rigidly fixed by having the subjects bear down on a bite block that was attached to a table by a rigid steel arm. The recorded current measurements and computer simulations were done independently so that the investigators were blind to the outcomes until the correlations were calculated.

Experiment 2: individual recordings

Subjects

In the second study, 18 additional volunteer adult subjects aged from 21 to 68 years (10 males and 8 females) without known anatomical abnormalities were

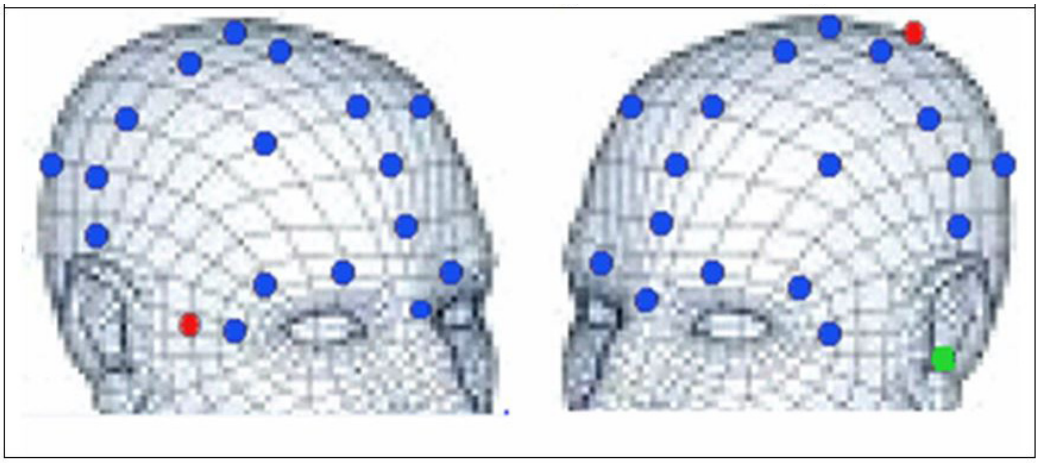

Fig. 2 **The images represent the locations used in recording the stimuli from the head in experiment 1.** The blue dots represent the recording sites for validation of the model. The red dots represent the stimulating electrodes used in experiment 1. The green dot is the location of the ground electrode.

recruited for imaging and analysis. Subjects´ MRI data were recorded by using the Aaken Insite protocol (see MRI procedures above). Seventy-five brain regions were identified by semi-automated segmentation (image 1), visually reviewed and corrected, and current densities were simulated and analyzed for each of 4 electrode configurations: F8-P2, C3-C4, F8-F7 and Fpz-O1.

Segmentation

Segmentation was achieved with a multi-step approach that used a combination of automated systems and manual scribing and correction. The automated analysis is described in detail in the study of Pierson et al.[44]. Briefly, the scans were processed through AutoWorkup[45], an automated procedure implemented with BRAINS[44,45]. The T1 image was reoriented by stepwise co-registration using BRAINSfit[46] to a set of template images, and then using the result of each co-registration as the initialization for the next step. The anterior commissure (AC point) was set to be the center of the image, and the scan was recorded at a 1 mm resolution in a $256\times256\times256$ matrix. The T2 image was then co-registered to the final T1 image and resampled to the same size and resolution. By using an intracranial mask to define the region of interest, each of the modalities underwent inhomogeneity correction by using ITKN4 (an image registration and segmentation toolkit). The final images were intensity normalized to map all regions inside the brain to intensities from 0 to 255.

Tissue classification[47] was then completed by using both modalities, a new brain mask was generated and cleaned, and the Talairach bounds of the cortex were automatically determined. Probability maps of the hippocampus and amygdala, used as input to artificial neural network software[48], were warped to the individual scans. The artificial neural networks were applied to each scan to identify these regions on each subject. The hypothalamus and pituitary were manually traced by using the T1 and continuous classified images. The skull-stripped, inhomogeneity corrected T1 images were then used as input to FreeSurfer (version 5.1)[49]. The 3-D segmentations of the cortical regions (aparc) from FreeSurfer were then co-registered into the BRAINS´ AutoWorkup image space and a code image including all of these segmented regions was created. Results were visually inspected and edited as necessary for accuracy. The images in ***Fig. 3*** show the location and shape of the cortical segmentations. The modeled stimulating electrodes which were placed according to the 10-20 system were F8-P2, C3-C4, F8-F7 and Fpz-O1. The virtual electrodes were a single voxel in size.

Statistical analysis

Statistical analysis was performed by using Xlstat software (Addinsoft, New York, NY, USA). The Pearson product-moment correlation coefficient was used in the validation experiment to compare measured and modeled voltages. Variability of current density values in ***Fig. 8*** are presented as box charts with whisker plots. The top of the whisker is the maximum current density for a subject; the bottom of the whisker is the minimum current density. The top of the box is the third quartile, and the bottom of the box is the first quartile. The diamond represents the mean value, and the line represents the median value.

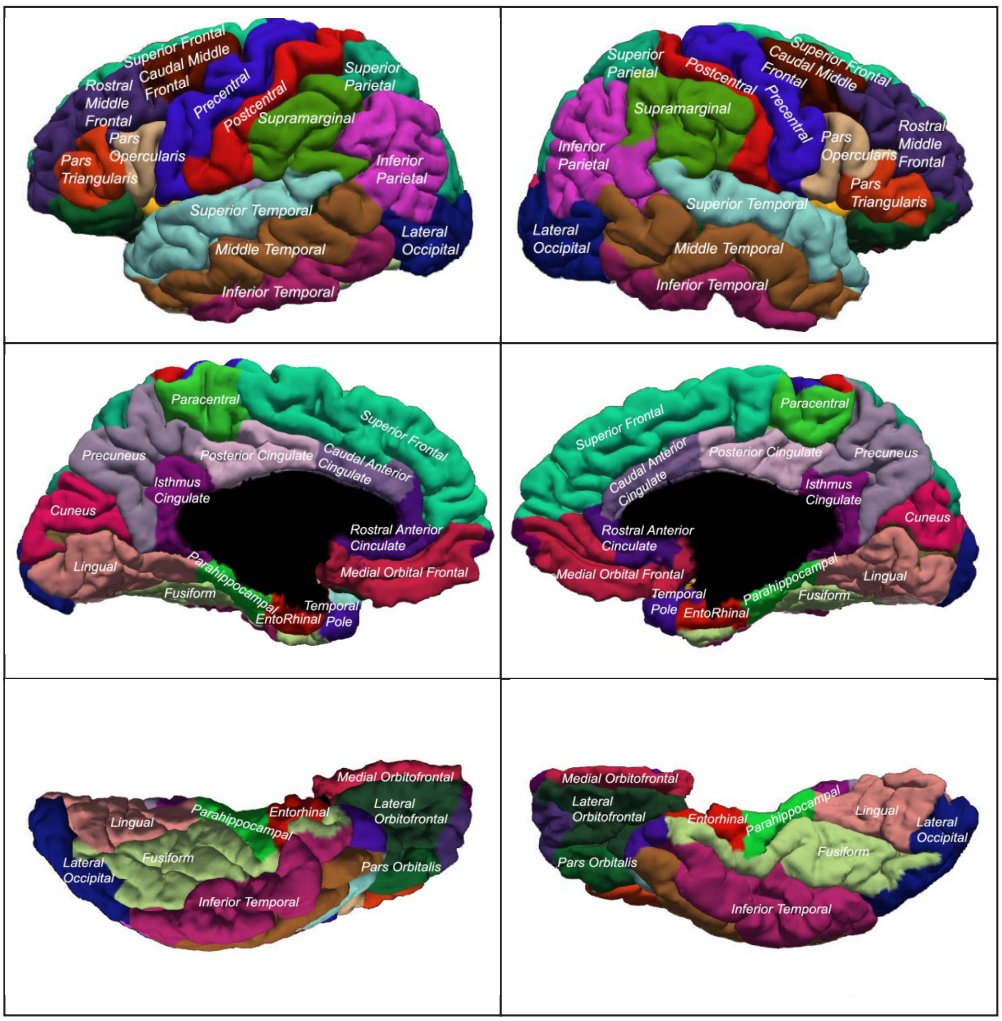

Fig. 3 **The illustrations show the names and regions used in the cortical segmentation regions for experiment 2.**

RESULTS

Experiment 1: validation

Pearson R values of the subjects´ calibration results were 0.91, 0.92 and 0.96. ***Fig. 4*** shows the subject points for both the measured and modeled voltages at 25 identical locations on the surface of a head, and suggests close correlations between the subject measurements and the simulation. ***Fig. 5*** shows the distribution of tissues and an intensity histogram with their relative resistivity values represented in color. ***Fig. 6*** uses the same colors against the combined gray image to better illustrate the types of tissues that are predominate and the amount of overlap within a tissue type. The overlap reflects the fact that tissues types are not homogeneous, and more than one tissue type may be present within a voxel.

Experiment 2: individual recordings

There was significant variability between subjects in all regions of the brain. The greatest variance was in the cortical structures (***Table 1***, ***Fig. 7*** and ***8***) with generally less variability in the subcortical areas. All examined areas received some amount of current. The 5 areas with the largest and least variability are listed for each electrode configuration in ***Table 1***. Some areas show as much as 6 to 10 fold difference between subjects. The right pars orbitalis with the F8-P2 stimulation showed a 5-107 μA/cm^2 range of response.

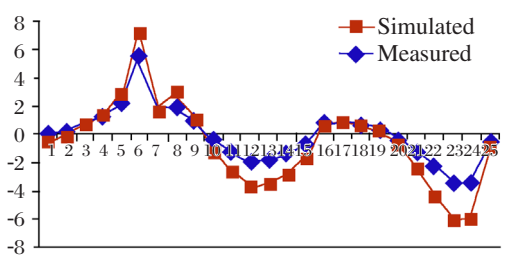

Fig. 4 **Results of 25 modeled and 25 measured values taken from the surface of the head.** The correlation between the values was r = 0.96.

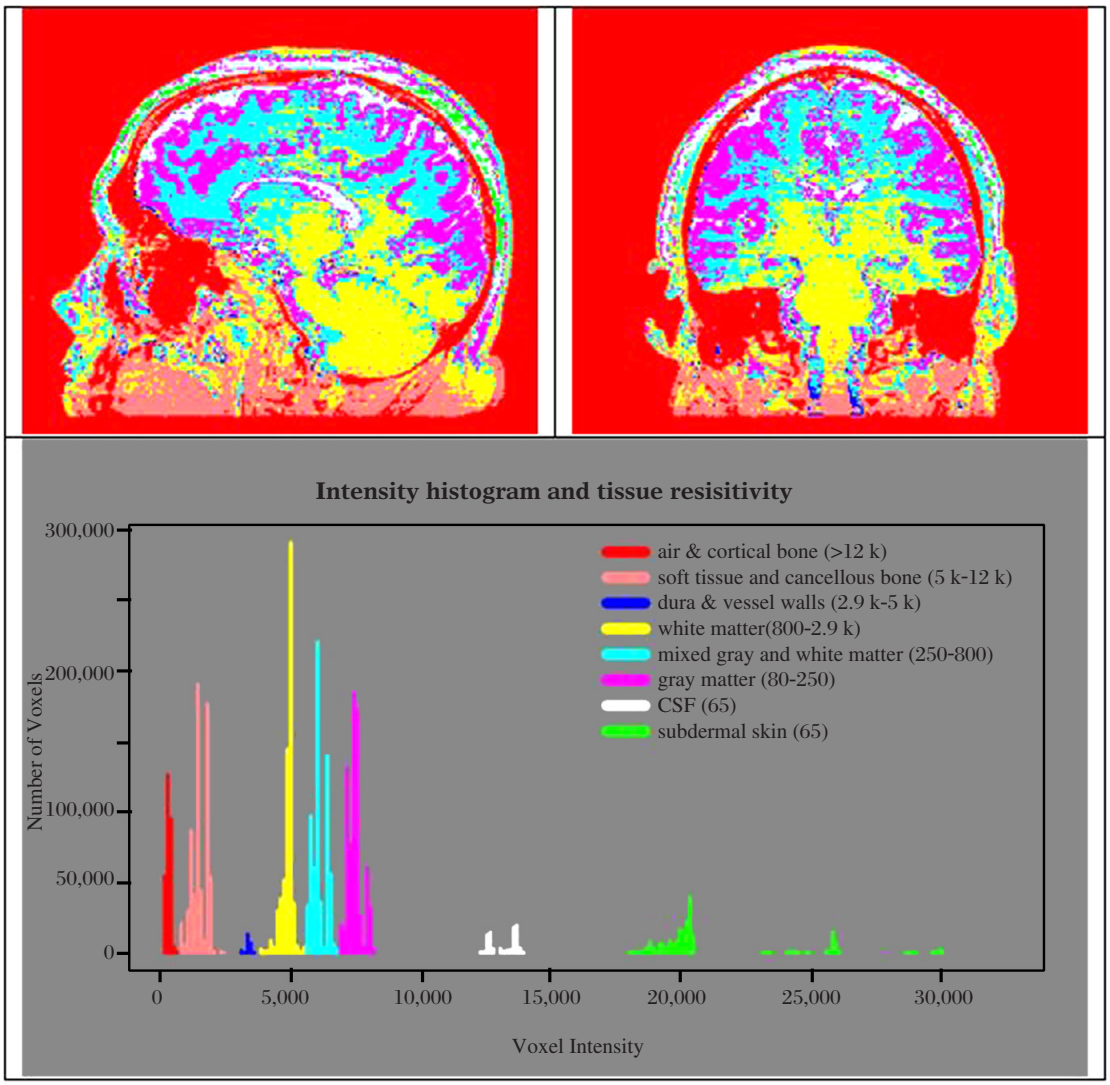

Fig. 5 **Color coded images of the various tissues and histogram of the number of voxels at each range of combined MRI intensity converted to color maps of resistivity.** Note that the resistivities overlap different types of tissues and vary somewhat within tissues. The colors represent the tissues in a range of resistive values in Ohms per centimeter.

Generally, cortical regions near the electrodes had the largest current density values, but also the greatest individual variation. Regions of the brain that are distant from the electrical stimulus in all 4 stimulus configurations, such as the pituitary gland and the hypothalamus, had significant levels of current density (mean levels for the pituitary were: F8-P2 = 3.1, C3-C4 = 1.8, F7-F8 = 4.8 and FPz-O1= 3.3 μA/cm^2).

The highest current levels and greatest variance were found with the right F8-P2 stimulation (***Table 1***, ***Fig. 7*** and ***8***). The highest levels within a structure were found in the right pars orbitalis, right pars triangularis and right precentral. In most instances, the areas with the lowest values also had the lowest variance and were most distant from the stimulating electrodes. This was particularly true when the electrodes were placed close together. As might be expected that the C3-C4 and F7-F8 electrode positions had the lowest values overall and least variance in those regions that were distant from the electrodes. However, there were exceptions to this distance rule. Regions where high- and low-resistivity tissues bordered each other often showed surprisingly high current densities and variance. These "hot spots" were difficult to predict and variance within segmented regions could often equal that seen between segmented regions. Even areas with the lowest variance typically showed a two-fold or greater difference between subjects (***Table 1***).

The cortical variability appeared to be largely dependent on the local architecture of the cranium and skull thickness. Small anomalies such as vessels pass-

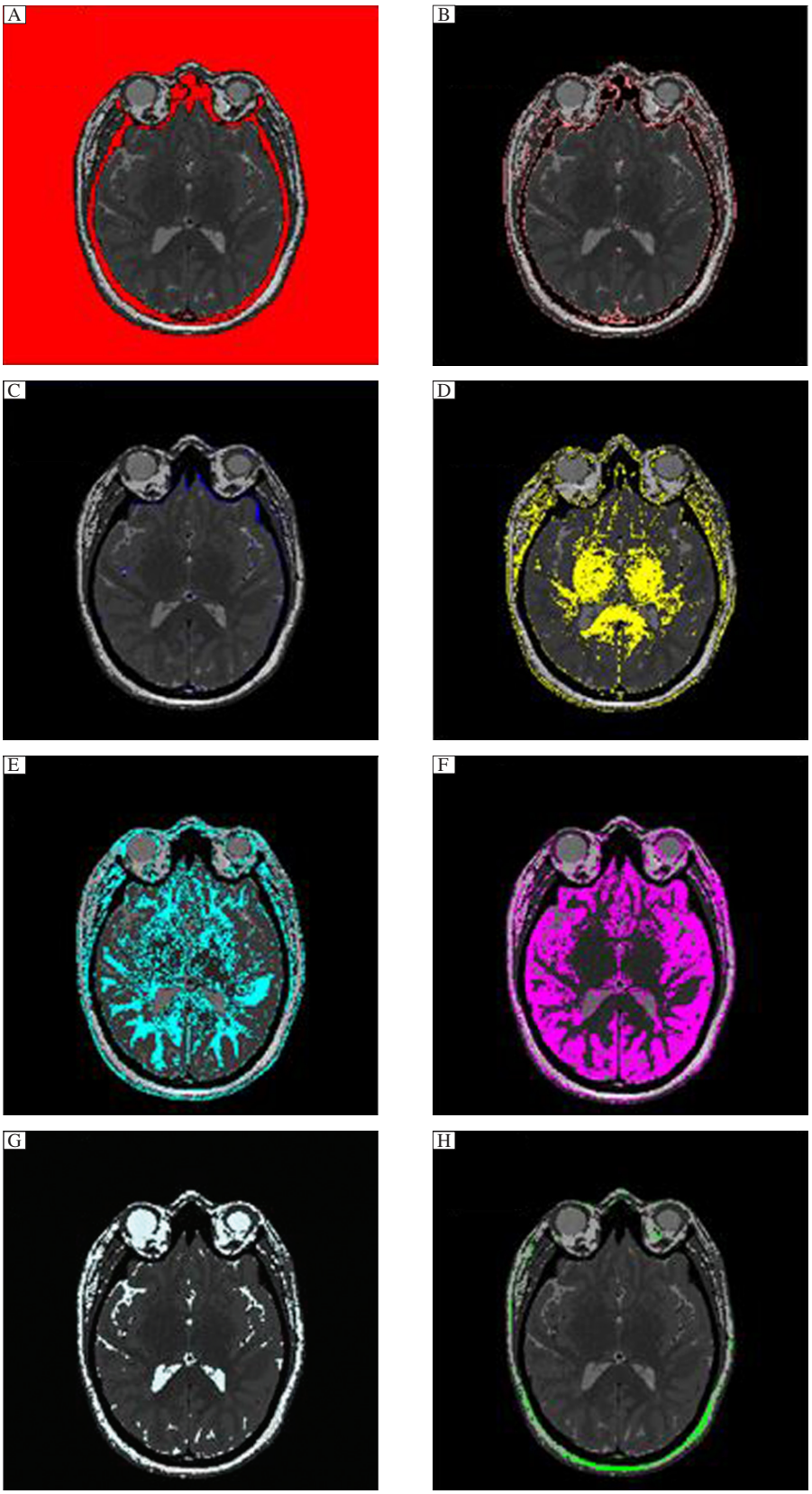

Fig. 6 **Axial slices with only one range of resistivity colored against a combined gray image to illustrate the types of tissues that are included for each range of resistivity.** Note that there is some overlap between tissue types. A = cortical bone and air, B = soft tissue, C = dura and vessel walls, D = white matter, F = grey matter, G = spinal fluid, H = subdermal skin.

Table 1 **Values from the segmented structures with the five highest and five lowest values for each of the electrode locations**

Segmentations with the highest variance					
C3-C4	L. Postcentral 5.4-34.9	L. Superior Parietal 6.9-29.8	R. Postcentral 5.5-35.9	R. Precentral 5.5-26.8	R. Superior Parietal 6.6-29.4
F7-F8	L. Pars Opercularis 3.7-30.0	L. Pars Triangularis 7.4-39.7	L.Rostral Middle Frontal 7.7-43.0	R.Pars Opercularis 3.6-27.7	R.Pars Triangularis 7.5-43.2
FPz-O1	L. Frontal Pole 3.4-26.3	L. Pars Triangularis 5.5-28.4	L. Superior Frontal 5.7-26.2	R. Frontal Pole 2.8-31.0	R. Peri-calcarine 4.0-26.2
F8-P2	L. Frontal Pole 3.0-29.2	R. Pars Opercularis 5.2-25.2	R. Pars Orbitalis 4.9-106.8	R. Pars Angularis 6.0-66.3	R. Postcentral 7.0-37.6
Segmentations with the lowest variance					
C3-C4	L. Middle Temporal 2.0-4.7	L. Parahippocampal 1.4- 3.4	L. Posterior Cingulate 6.2-11.9	L. Rostral Middle Frontal 4.6-11.5	R. Middle Temporal 2.2-5.8
F7-F8	L. Inferior Parietal 3.2-6.2	L. Inferior Temporal 2.3-5.1	R. Middle Temporal 3.1-6.2	R. Superior Temporal 2.9-5.8	R. Supramarginal 4.5-9.2
FPz-O1	L. Entorhinal 2.6-6.7	L. Parahippocampal 3.4-7.4	R. Fusiform 3.9-7.4	R. Parahippocampal 4.4-8.1	R. Superior Temporal 7.1-13.2
F8-P2	L. Amygdala 2.2-5.6	L. Fusiform 1.7-4.1	L. Temporal Pole 1.4-5.4	R. Lingual 1.6-4.2	R. Pericalcarine 1.8-5.6

The table shows the values from the segmented structures with the five highest and five lowest values for each of the electrode locations. The values are $\mu A/cm^2$. The complete data set is too extensive for publication here, but the complete data set is available by E-mail request at: mrussell@aakenlabs.com.

ing through the skull and the presence or absence of cancellous bone significantly impacted the current levels especially near the electrodes. The presence of cerebral spinal fluid in sulci or ventricles appeared to draw the current into the brain cavities, but a gyrus had the opposite effect. This can be explained by the low resistivity of spinal fluid providing a favored path for electrical current and the high resistivity of dura and bone forcing the current into alternate paths.

It appears that when electrodes are placed on the scalp, there is a series of tissue layers constrict and expand the current distribution. The sub-dermal skin, which is a good conductor, allows current to expand over the lesser conducting bone. Cerebral spinal fluid beneath the bone spreads the current out again and the dura (a poor conductor) constricts the current. These layers play a significant role in initial current distribution before the complex brain anatomy further distributes the current.

DISCUSSION

The variability at regions near or under the electrodes is significant as these are the regions that are usually targeted for cortical stimulation. Investigators conventionally assume that subjects are receiving similar amounts of current when electrodes are placed directly over the targeted site. However, the present study indicated that while higher current density tends to occur in regions near electrodes, there is a significant variation between subjects. While areas distant from the electrodes generally have less variability, the differences are still substantial. This is particularly true of regions that border high- and low-conducting tissues (e. g. cerebrospinal fluid and meninges) or along conductive pathways such as vessels or down axonal bundles. These regions show significant variation and often have multiple areas of high- and low-density current (***Fig. 7*** and ***8***).

TCES with the C3-C4 configuration is extensively used to elicit motor evoked potentials from the legs and feet, and is the primary means of assessing the integrity of the motor pathways during spinal cord surgery[11-13]. This monitoring procedure typically uses pulse trains of up to 400 volts. Thousands of patients undergo this procedure every year with the assumption that the only effect is on the motor pathways. Data from this study suggested that other areas of the brain maybe receiving large current densities simultaneously including the anterior cingulate, an area commonly targeted in depression[50-52]. The effects of these additional stimulations are not known.

TCES with the right-temporal to P2 configuration is one of the standard lead placements for the electroconvulsive shock therapy treatments (Brunoni, Teng, 2010, Martin, 1986). A significant degree of variation in the clinical outcomes from this stimulation has been consistently reported[53,54]. Data in this study suggests that some of the inconsistencies in clinical results may

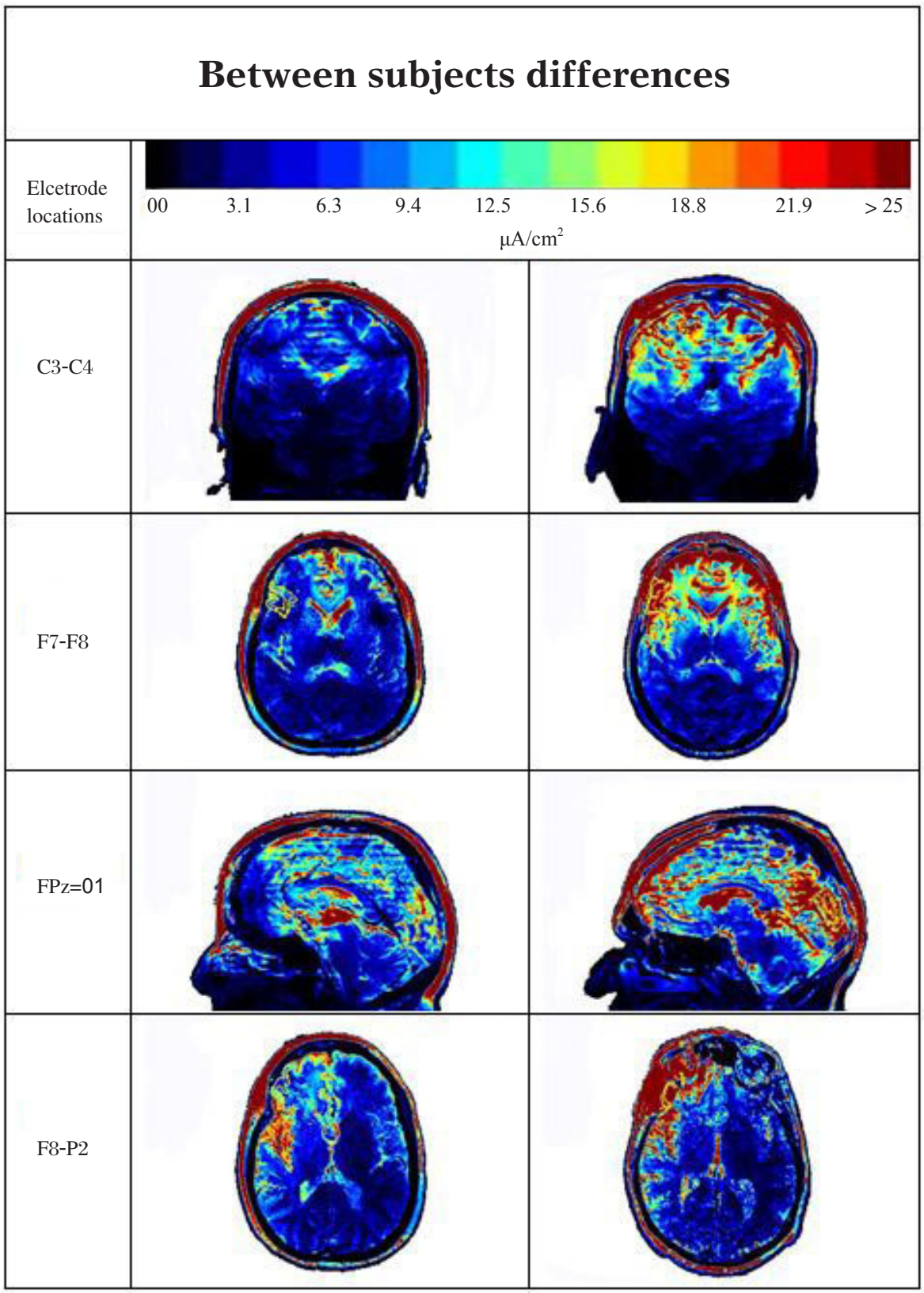

***Fig. 7* Variability between subjects in all regions of the brain.** The images illustrate individuals with different current distributions for each of the 10-20 positions shown on the left column. The red indicates high current density and the blue low current density.

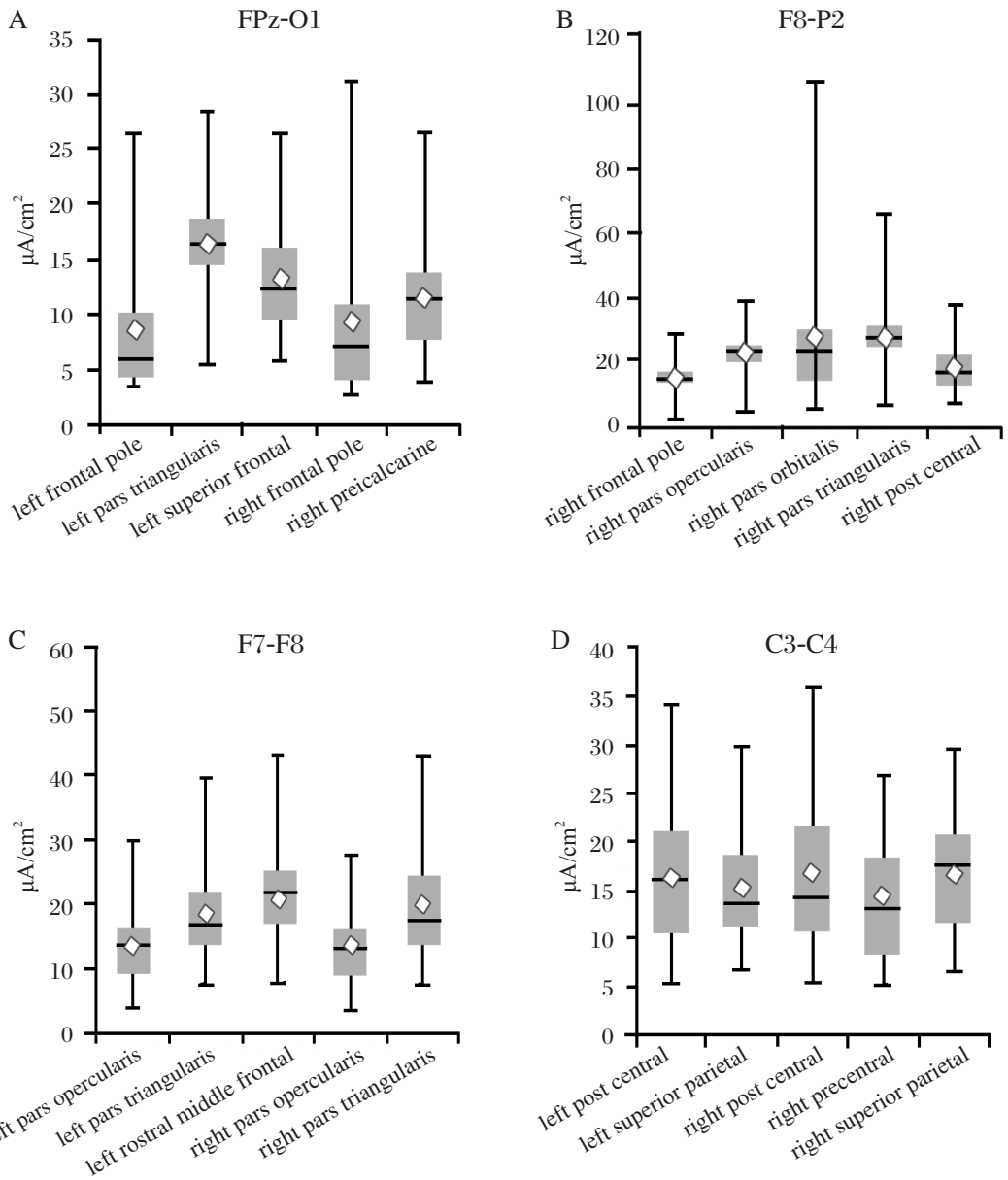

Fig. 8 **The box charts and whisker plots show the five areas with the highest level of variance for each of the electrode locations.** The top of the whisker is the maximum current density for a subject; the bottom of the whisker is the minimum current density. The top of the box is the third quartile, and the bottom of the box is the first quartile. The diamond represents the mean value, and the line represents the median value. Note that each chart has a different scale. Seventy five regions were analyzed for each electrode pair and the results are too numerous to present here. Complete data sets are available by Email from: mrussell@aakenlabs.com.

be due to variability in amount of current actually received by targeted brain regions. Sackeim[56] and a number of others[57-59] have suggested that focally administered electrical current has the potential to improve treatment and reduce side effects of electroconvulsive treatments. Individualized targeting will likely further improve outcomes.

Compared to the traditional method of selecting stimulus locations by measuring landmarks on the scalp, modeling electrical stimulation may be a superior tool for treatment planning to determine both the optimal electrode location and current density delivered to specific regions for a subject[35,57–,59] TCES modeling will be helpful in more accurately targeting specific regions and in avoiding adverse side effects. For applications where accuracy of stimulus delivery is a consideration, it offers a possible alternative for determining electrode placement to the traditional 10-20 system. Future work will focus on examining how modifying electrode placements to accommodate

individual differences in head anatomy can more precisely target areas of the brain.

The limitations of this study is as follows: the direct measurement of current in the first experiment and close correlations of the modeling outcomes are supportive of the modeling´s accuracy and providing confidence in the general outcomes. However, measurements from in depth structures have not been made and may vary from what is illustrated here, and are the focus of current research. Internal validation of the study is underway, but has not been completed. There is some slight variation in the values measured in experiment 1 between the modeled values and the measured values. It is not clear that if this divergence is due to an error in the model or to the difficulty of making precise electrical measurements from the scalp. Nevertheless, the correlations are quite good and support the premise that MRIs can be used to model resistivity.

Values determined through the modeling will change if the subject´s condition changes. If swelling or hemodynamic changes occur between MRI capture and when the simulation is applied, these values may also change. Although the electrical stimulation modeled herein was 2mA, the results may be extrapolated to somewhat different current strengths for DC and low frequency alternating current (AC) stimulation[60] by the application of Ohm´s law. Extrapolation should be done with caution, however, because AC stimulation is influenced by the capacitance of the cranial tissues, and DC stimulation that is left on for extended periods of time will likely change the properties of the tissues due to electrolytic instabilities.

This study is also limited by the quality and resolution of the MRI. Any noise, error, or artifact that exists in the MRI will be reflected in the modeling. While the modeling made adjustments for the anisotropic properties of the tissues, the resolution of MRI is limited by the voxel size. Thus, conductivity value within a voxel is a mean value of all entities within the voxel and does not represent the fine architecture of the tissues within the voxel. A voxel may contain many nerve fibers or a combination of nerve fibers and fine blood vessels. There is a high degree of variation in conductivity between myelinated fibers, unmyelinated fibers and interstitial spaces. This analysis is not capable of showing that level of resolution as the MRI is not able to distinguish subjects´ neurons. As the resolution of MRIs improves, the quality of the modeling will also improve.

Electrical modeling of the head should find applications in a variety of clinical and research applications. The values here were presented in microamperes per square centimeter, but the values can be converted to represent different electrical units or intensities.

While the focus here was in individual variation, there was also significant variation seen within structures and those values will be reported in a subsequent publication. The values provided here were means for the segmentations and a finer analysis may be desirable for specific regions within these structures.

In conclusion, when electrodes are placed on the scalp, current pathways are determined by the complex anatomy of the head and the individual resistivities of the various tissues. MRIs are capable of representing this complexity if the MRI is recorded as a measurement of the level of hydrogen within tissues, and the hydrogen is regarded as a way for determining the amount of conductive fluid within a tissue. Recorded measurements taken from the scalp closely correspond with predicted values anticipated by the modeling. Common configurations for the placement of electrodes on the scalp for clinical practice have very diverse distributions of current within the subjects´ brain and very divergent intensity levels between subjects. The development of a technique for modeling current densities implies that more accurate targeting of brain areas for stimulation are possible for both research and clinical practice. MRI based modeling may be a more desirable method of determining electrode placement and stimulation intensity than the 10-20 system or other methods based on scalp topography when accurate targeting of brain structures is needed.

Acknowledgements

This research was supported by the Sutter Institute for Medical Research, and the Aaken Research Institute. We thank Radiological Associates of Sacramento and David Seidenwurm for help with the MRI data collection and Rosalind Sadleir at the University of Florida at Gainesville for her help with the finite element analysis. We used ITK-Snap for preparation of ***Fig. 5***, and Statistical R for the histogram in ***Fig. 6***.

References

[1] Bikson M, Bulow P, Stiller JW, Datta A, Battaglia F, Karnup SV, et al. Transcranial direct current stimulation for major depression: a general system for quantifying transcranial electrotherapy dosage. *Curr Treat Options Neurol* 2008; 10: 377-85.

[2] Boggio PS, Rigonatti SP, Ribeiro RB, Myczkowski ML, Nitsche MA, Pascual-Leone A, et al. A randomized, double-blind clinical trial on the efficacy of cortical direct current stimulation for the treatment of major depression. *Int J Neuropsychopharmacol* 2008; 11: 249-54.

[3] Brunoni AR, Teng CT, Correa C, Imamura M, Brasil-Neto JP, Boechat R, et al. Neuromodulation approaches for the treatment of major depression: challenges and

recommendations from a working group meeting. *Arq Neuropsiquiatr* 2010; 68: 433-51.

[4] George MS, Nahas Z, Li X, Kozel FA, Anderson B, Yamanaka K, et al. Novel treatments of mood disorders based on brain circuitry (ECT, MST, TMS, VNS, DBS]. *Semin Clin Neuropsychiatry* 2002; 7 :293-304.

[5] Frank E, Schecklmann M, Landgrebe M, Burger J, Kreuzer P, Poeppl TB, et al. Treatment of chronic tinnitus with repeated sessions of prefrontal transcranial direct current stimulation: outcomes from an open-label pilot study. *J Neurol* 2012; 259: 327-33.

[6] Seidman MD, Ridder DD, Elisevich K, Bowyer SM, Darrat I, Dria J, et al. Direct electrical stimulation of Heschl´s gyrus for tinnitus treatment. *Laryngoscope* 2008;118: 491-500.

[7] Vanneste S, Plazier M, Ost J, van der Loo E, Van de Heyning P, De Ridder D. Bilateral dorsolateral prefrontal cortex modulation for tinnitus by transcranial direct current stimulation: a preliminary clinical study. *Exp Brain Res* 2010; 202: 779-85.

[8] Terney D, Chaieb L, Moliadze V, Antal A, Paulus W. Increasing human brain excitability by transcranial high-frequency random noise stimulation. *J Neurosci* 2008; 28: 14147-55.

[9] Utz KS, Dimova V, Oppenlander K, Kerkhoff G. Electrified minds: transcranial direct current stimulation (tDCS) and galvanic vestibular stimulation (GVS) as methods of non-invasive brain stimulation in neuropsychology--a review of current data and future implications. *Neuropsychol* 2010; 48: 2789-810.

[10] Paulus W. Outlasting excitability shifts induced by direct current stimulation of the human brain. *Suppl Clin Neurophysiol* 2004; 57: 708-14.

[11] Chiappa KH. Transcranial motor evoked potentials. *Electromyography Clinical Neurophysiol* 1994; 34: 15-21.

[12] MacDonald DB. Safety of intraoperative transcranial electrical stimulation motor evoked potential monitoring. *J Clin Neurophysiol* 2002; 19: 416-29.

[13] Sutter M, Eggspuehler A, Muller A, Dvorak J. Multimodal intraoperative monitoring: an overview and proposal of methodology based on 1,017 cases. *Euro Spine J* 2007; 16 Suppl 2: S153-61.

[14] Kellner CH, Greenberg RM, Murrough JW, Bryson EO, Briggs MC, Pasculli RM. ECT in treatment-resistant depression. *Am J Psychiatry* 2012; 69: 1238-44.

[15] Sommer IE, Slotema CW, Daskalakis ZJ, Derks EM, Blom JD, van der Gaag M. The treatment of hallucinations in schizophrenia spectrum disorders. *Schizophr Bull* 2012; 38: 704-14.

[16] Dierckx B, Heijnen WT, van den Broek WW, Birkenhäger TK. Efficacy of electroconvulsive therapy in bipolar versus unipolar major depression: a meta-analysis. *Bipolar Disord* 2012; 14: 146-50.

[17] Fregni F, Boggio PS, Lima MC, Ferreira MJ, Wagner T, Rigonatti SP, et al. A sham-controlled, phase II trial of transcranial direct current stimulation for the treatment of central pain in traumatic spinal cord injury. *Pain* 2006; 122: 197-209.

[18] Fregni F, Freedman S, Pascual-Leone A. Recent advances in the treatment of chronic pain with non-invasive brain stimulation techniques. *Lancet Neurol* 2007; 6: 188-91.

[19] Javadi AH, Cheng P, Walsh V. Short duration transcranial direct current stimulation (tDCS) modulates verbal memory. *Brain Stimul* 2012; 5: 468-74.

[20] Zaehle T, Sandmann P, Thorne JD, Jancke L, Herrmann CS. Transcranial direct current stimulation of the prefrontal cortex modulates working memory performance: combined behavioural and electrophysiological evidence. *BMC Neurosci* 2011; 12: 2.

[21] Nitsche MA, Paulus W. Noninvasive brain stimulation protocols in the treatment of epilepsy: current state and perspectives. *Neurotherapeutics* 2009; 6: 244-50.

[22] Feng JF, Liu J, Zhang XZ, Zhang L, Jiang JY, Nolta J, et al. Guided migration of neural stem cells derived from human embryonic stem cells by an electric field. *Stem Cells* 2012; 30: 349-55.

[23] Lefaucheur JP. Methods of therapeutic cortical stimulation. *Neurophysiol Clin* 2009; 39: 1-14.

[24] Song B, Gu Y, Pu J, Reid B, Zhao Z, Zhao M. Application of direct current electric fields to cells and tissues in vitro and modulation of wound electric field *in vivo*. *Nature Protocol* 2007; 2: 1479-89.

[25] Tai G, Reid B, Cao L, Zhao M. Electrotaxis and wound healing: experimental methods to study electric fields as a directional signal for cell migration. *Methods Mol Biol* 2009; 571: 77-97.

[26] Zhao M, Penninger J, Isseroff RR. Electrical Activation of Wound-Healing Pathways. *Adv Skin Wound Care* 2010;1:567-73.

[27] Zheng X, Alsop DC, Schlaug G. Effects of transcranial direct current stimulation (tDCS) on human regional cerebral blood flow. *Neuroimage* 2011; 58: 26-33.

[28] Kirson ED, Dbaly V, Tovarys F, Vymazal J, Soustiel JF, Itzhaki A, et al. Alternating electric fields arrest cell proliferation in animal tumor models and human brain tumors. *PNAS* 2007; 104: 10152-7.

[29] Faber M, Vanneste S, Fregni F, De Ridder D. Top down prefrontal affective modulation of tinnitus with multiple sessions of tDCS of dorsolateral prefrontal cortex. *Brain Stimul* 2012; 5: 492-8.

[30] Holdefer RN, Sadleir R, Russell MJ. Predicted current densities in the brain during transcranial electrical stimulation. *Clin Neurophysiol* 2006; 117: 1388-97.

[31] Lee WH, Deng ZD, Laine AF, Lisanby SH, Peterchev AV. Influence of white matter conductivity anisotropy on electric field strength induced by electroconvulsive therapy. *Conf Proc IEEE Eng Med Biol Soc* 2011; 2011: 5473-6.

[32] Mendonca ME, Santana MB, Baptista AF, Datta A, Bikson M, Fregni F, et al. Transcranial DC stimulation in fibromyalgia: optimized cortical target supported by high-resolution computational models. *J Pain* 2011; 12:

610-7.

[33] Sadleir RJ, Vannorsdall TD, Schretlen DJ, Gordon B. Transcranial direct current stimulation (tDCS) in a realistic head model. *Neuroimage* 2010; 51: 1310-8.

[34] Salvador R, Mekonnen A, Ruffini G, Miranda PC. Modeling the electric field induced in a high resolution realistic head model during transcranial current stimulation. *Conf Proc IEEE Eng Med Biol Soc* 2010; 2010: 2073-6.

[35] Datta A, Elwassif M, Battaglia F, Bikson M. Transcranial current stimulation focality using disc and ring electrode configurations: FEM analysis. *J Neural Eng* 2008; 5: 163-74.

[36] Im CH, Jung HH, Choi JD, Lee SY, Jung KY. Determination of optimal electrode positions for transcranial direct current stimulation (tDCS). *Phys Med Biol* 2008; 53: N219-25.

[37] Wagner T, Fregni F, Fecteau S, Grodzinsky A, Zahn M, Pascual-Leone A. Transcranial direct current stimulation: a computer-based human model study. *Neuroimage* 2007; 35: 1113-24.

[38] Westerbrook C KRC, Talbot J. MRI in Practice 3rd ed. 3rd ed. Oxford: Blackwell 2005.

[39] Faes TJ, van der Meij HA, de Munck JC, Heethaar RM. The electric resistivity of human tissues (100 Hz-10 MHz): a meta-analysis of review studies. Physiol. *Measure* 1999; 20: R1-10.

[40] Gullmar D, Gaueisen J, Reichenbach JR. Influence of anistropic conductivity. *Neuroimage* 2010; 51: 145-63.

[41] Russell MJ. Guided Electrical Transcranial Stimulation (GETS) Technique. In: USPTO, editor. *United States* 2006.

[42] Davies AJ. The finite element method: a first approach. Oxford: Clarendon Press; 1980.

[43] Press WH. Numerical recipes in pascal: the art of scientific computing Cambridge: Cambridge University Press; 1989.

[44] Pierson R, Johnson H, Harris G, Keefe H, Paulsen JS, Andreasen NC, et al. Fully automated analysis using BRAINS: AutoWorkup. *Neuroimage* 2011; 54: 328-36.

[45] Pierson R,Harris G, Hohnson J, Dunn S, Magnotta VA. Maximize uniformity summation heuristic (MUSH): a highly accurate simple method for intracranial delineation. In: Pluim J. DB, editor. Mediocal Imaging: 2009 Image Processin Bellingham, WA SPIE: 2009.

[46] Johnson H, Harris G, Williams K. BRAINSFit: Mutual information registration of whole-brain 3D images, using the insight toolkit. *Insight J* 2007; 1: 1-7.

[47] Harris G, Andreasen NC, Cizadlo T, Bailey JM, Bockholt HJ, Magnotta VA, et al. Improving tissue classification in MRI: a three-dimensional multispectral discriminant analysis method with automated training class selection. *J Cmputer Assisted Tomog* 1999; 23: 144-54.

[48] Powell S, Magnotta VA, Johnson H, Jammalamadaka VK, Pierson R, Andreasen NC. Registration and machine learning-based automated segmentation of subcortical and cerebellar brain structures. *Neuroimage* 2008; 39: 238-47.

[49] Fischl B, Liu A, Dale AM. Automated manifold surgery: constructing geometrically accurate and topologically correct models of the human cerebral cortex. IEEE Trans. Med. Imag. 2001; 20: 70-80.

[50] Hamani C, Mayberg H, Stone S, Laxton A, Haber S, Lozano AM. The subcallosal cingulate gyrus in the context of major depression. *Biol Psychiatry* 2011; 69: 301-8.

[51] Lozano AM, Giacobbe P, Hamani C, Rizvi SJ, Kennedy SH, Kolivakis TT, et al. A multicenter pilot study of subcallosal cingulate area deep brain stimulation for treatment-resistant depression. *J Neurosurg* 2012; 116: 315-22.

[52] Mayberg HS, Lozano AM, Voon V, McNeely HE, Seminowicz D, Hamani C, et al. Deep brain stimulation for treatment-resistant depression. *Neuron* 2005; 45: 651-60.

[53] Martin BA. Electroconvulsive therapy: contemporary standards of practice. *Canad J Psychiatry Rev Canade Psychi* 1986; 31: 759-71.

[54] Dombrovski AY, Mulsant BH. The evidence for electroconvulsive therapy (ECT) in the treatment of severe late-life depression. ECT: the preferred treatment for severe depression in late life. Internat Psychogeriatrics / IPA. 2007; 19: 10-4, 27-35; discussion 24-6.

[55] McClintock SM, Brandon AR, Husain MM, Jarrett RB. A systematic review of the combined use of electroconvulsive therapy and psychotherapy for depression. *J ECT* 2011; 27: 236-43.

[56] Sackim H. Convulsant and anticonvulsant propeties of electroconvulsive therapy:towards a focal form of brain stimulation. *Clin Neurosci Researh* 2004; 4: 39-57.

[57] Lee WH, Deng ZD, Kim TS, Laine AF, Lisanby SH, Peterchev AV. Regional electric field induced by electroconvulsive therapy in a realistic finite element head model: influence of white matter anisotropic conductivity. *Neuroimage* 2012; 59: 2110-23.

[58] Spellman T, Peterchev AV, Lisanby SH. Focal electrically administered seizure therapy: a novel form of ECT illustrates the roles of current directionality, polarity, and electrode configuration in seizure induction. *Neuropsychopharmacol* 2009; 34: 2002-10.

[59] Kmochowski JP, Datta A, Bikson M, Su Y, and Parra LC. Optimized mulit-electrode stimulation increases focality and intensity at the target. *J Neural Eng* 2011; 8: 046011.

[60] Gabriel C, Peyman A, Grant EH. Electrical conductivity of tissue at frequencies below 1 MHz. *Physics Med Biol* 2009; 54: 4863-78.